Supplementary Information for

Plenty of motion at the bottom: Atomically thin liquid gold membrane

Authors: Pekka Koskinen[1]* and Topi Korhonen[1]

Affiliations:

[1]Nanoscience Center, Department of Physics, University of Jyvaskyla, 40014 Jyväskylä, Finland.

*Correspondence to: pekka.koskinen@iki.fi

Materials and Methods:

Density-functional theory (DFT) simulations – We used the exchange-correlation functional of Perdew, Burke, and Ernzerhof and the real-space grid DFT code GPAW (*43–45*). The code was used in the local basis mode (LCAO) with a double-zeta polarized basis, which speeded up the computations but still gave accuracy comparable to the full grid for our purposes. Grid spacing was 0.2 Å, Fermi broadening was 0.05 eV, and the k-space was sampled at the Γ-point. The vertical dimensions in the simulation cells were non-pediodic and their lengths were 16 Å. The lattice constant for infinite and close-packed 2D Au was 2.8 Å. Relativistic DFT simulations used the standard projector augmented wave (PAW) setups generated by scalar-relativistic calculation of the Au atom, as usual (*46*). Nonrelativistic DFT simulations used PAW setups and LCAO basis functions that were generated by a similar procedure with default parameters, apart from the Au atom that was solved using nonrelativistic formalism.

Density-functional tight-binding (DFTB) simulations – DFTB derives its parametrizations directly from *ab initio* electronic structure methods without semi-empirical fitting (*47, 48*), and is the method of choice when long-running molecular dynamics simulations are required. The DFTB Au parametrizations, established earlier, turned out to provide a fair description of the electronic structure in small nanostructures (*22*). There are quantitative differences, but the accuracy suffices for our qualitative purposes. In particular, parametrizations faithfully reproduce the propensity for planar bonding, which originates from enhanced 5d-6s orbital hybridization caused by relativistic contraction of core orbitals. This planar bonding and its origin, known from experiments and explained by DFT calculations, are reproduced also by DFTB (Fig. S1) (*22, 26*). Relativistic DFTB simulations used the parametrizations of Ref. (*22*), generated by scalar-relativistic calculation of the Au atom, just as with PAW setup generation for DFT. The relativistic DFTB parametrization gave 2.9 Å for the lattice constant of infinite close-packed 2D Au. Nonrelativistic DFTB calculations used parametrizations that were generated by the standard procedure of Ref. (*48*), apart from the Au atom that was solved using nonrelativistic formalism (repulsion was fit to Au_2 dimer and Au bulk with a 2.9 Å cutoff).

The DFTB C parametrizations were adopted from Ref. (*47*) and Au-C parametrizations were made following the standard procedure of Ref. (*48*): The parameters for quadratic confinements were $r_0 = 2.52$ Å for Au and $r_0 = 1.41$ Å for C, and the repulsion (with 2.65 Å cutoff) was fitted to dimer (AuC) and Au-benzene (C_6H_5Au) structures of varying Au-C bond lenghts (with PBE-DFT energies). As benchmark examples, the adsorption energy of Au in graphene single vacancy was 3.4 eV in DFTB and 3.0 eV in DFT (*16*), and the adsorption energy of Au in the zigzag edge

of graphene was 3.9 eV in DFTB and 3.4 eV in DFT (*15*). The agreement is satisfactory, given that also DFT numbers are functional-dependent. For systems with both Au and C atoms we used self-consistent charge (SCC) DFTB (*49*). For systems with only Au we could use a non-SCC approach without compromising accuracy because charge transfer was so small.

Molecular dynamics (MD) simulations – MD simulations used a 2.5 fs time step (5 fs for systems with Au only) and a Langevin thermostat. The thermostat used a 5 ps damping time (proportional to the inverse of friction coefficient), which was sufficiently large to rid all thermostat-induced artifacts in the atomic diffusion (Fig. S2A). Regarding atom diffusion in the periodic 2D Au, the most critical parameter was the lateral size of the cell. A cell with 64 atoms (size 23.5 Å×20.4 Å) showed convergent behavior with respect to both diffusion and mean cohesion (Figs. S2, B and C). All 2D Au simulations begun with 25 ps equilibration and completed with 0.25 ns data collection. Diffusion constant D was calculated via mean square displacement $\langle r^2 \rangle = 4Dt$ for the selected set of atoms (*50*). The velocity autocorrelation

$$z(t) = \frac{\langle \vec{v}(t_0) \cdot \vec{v}(t - t_0) \rangle}{\langle \vec{v}(t_0) \cdot \vec{v}(t_0) \rangle},$$

where $\vec{v}(t)$ is the $3N$-dimensional velocity vector, was averaged over 50 randomized initial times t_0 within the given trajectory. The pair correlation function was calculated as $g(r) = \sum_{ij} \delta_d(r - r_{ij}) / (2\pi r \sigma)$, where σ is the atom density and $\delta_d(r)$ is a Gaussian with a broadening $d = 0.25$ Å.

Bending rigidity of 2D Au and Au-C interface –The bending rigidity of the 2D Au was calculated by three approaches. First, Au tubes with radii of curvature below $R = 1.2$ nm were calculated both by DFT and DFTB (10 k-points for a tube of 5.1 Å periodic length). DFTB appeared to give a reasonable, even if slightly underestimated bending rigidity of 2D Au membrane when compared to DFT (Fig. S3A). This is in line with Fig. 4 in the main text. Second, following the procedure of Refs. (*51*) and (*52*), revised periodic boundary conditions (RPBC) were used to simulate the bending of an infinite 2D Au (one-atom cell with 10×10 k-points)(*53*). Fitting to radii of curvature above 20 Å yields static bending modulus of 0.45 eV, and extrapolating to radii of curvature below 20 Å yields the energies of Au tubes in satisfactory agreement (considering that tubes contain finite-size effects absent in RPBC simulations). Third, RPBC approach with Au$_{64}$ was used to calculate the temperature-dependence of the bending modulus. The modulus at given temperature was calculated by fitting the R^{-2}-behavior to a set of 0.5 ns simulations at R =20, 30, 50, 100, and 200 Å. Strain contributions that arose from slow radial movement of the membrane were removed prior to the fitting (the elastic modulus of 2D Au was 5.71 eV/Å^2). As a result, the bending rigidity increased at the rate 0.1 meV/K upon increasing temperature (Fig. S3B). Bending rigidity of the molten phase was not calculated, because it would have required inaccessibly long simulations. The bending rigidity of Au-C interface, as estimated from a periodic slab calculation, was approximately the same as that of 2D Au (Fig. S4).

Size-dependent stability analysis for patches suspended in graphene pores – Following Ref. 12, the stability of patches was estimated by the energy difference of pore-suspended patch and a three-dimensional nanocluster. The energy difference of a square patch of edge length L and a cubic nanocluster with the same number of atoms is

$$\Delta E = L^2(\varepsilon_{2D} - \varepsilon_{3D})/A_0 + 4L\varepsilon_{if} - 6(V_0/A_0)^{\frac{2}{3}}L^{\frac{4}{3}}\varepsilon_{surf}$$

where (using DFTB values) $\varepsilon_{2D} = -3.3$ eV is the 2D binding energy per atom, $\varepsilon_{3D} = -3.6$ eV is the 3D binding energy per atom (FCC bulk), $A_0 = 7.3$ Å^2 is the area per atom in 2D, $V_0 = 23$ Å^3 is the volume per atom in 3D (FCC bulk), $\varepsilon_{if} = -0.7$ eV/Å is the binding energy of Au-C interface (averaged over few randomized interfaces), and $\varepsilon_{edge} = 0.08$ eV/Å^2 is the surface energy (average over different facets). At small sizes the patch is energetically favorable ($\Delta E < 0$) due to the interface energy that is negative and linear in L. At larger sizes the 3D cluster becomes increasingly more favorable because of the 3D bulk term. The critical size above which the 3D clusters become energetically more favorable ($\Delta E = 0$) occurs around $L \approx 20$ nm.

Curvature-dependent melting temperature – The effect of curvature on the melting temperature of 2D Au was investigated by simulating Au cage clusters with 18, 32, 50, and 72 atoms. Unlike carbon fullerenes, the biggest of these golden cage-like isomers are most likely metastable and thus not seen in experiments (*19, 54, 55*). However, MD simulations at various temperatures showed that within 0.1 ns the clusters retained their cage-like geometries even though they were in liquid phase at the same time (Fig. S5A). Moreover, cage-like clusters showed reduced melting temperatures, apparently because in a curved surface the atoms had more freedom to move towards the convex side and thus they could overcome diffusion barriers more easily. This decrease in the melting temperature turned out to be directly proportional to the curvature (Fig. S5B).
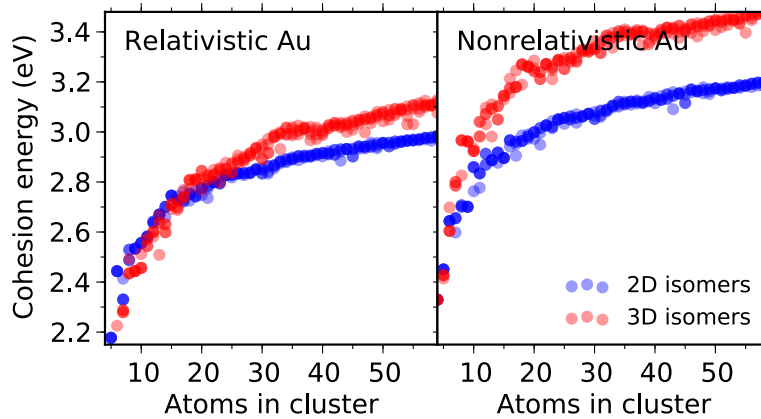
Figures S1-S5:

Fig. S1. The planar bonding trends in small gold clusters with DFTB. Relativistic (left) and nonrelativistic (right) calculations of the cohesive energy per atom for 2D and 3D low-energy cluster isomers from global optimization (few isomers shown for each cluster size). The transition from 2D to 3D ground state shifts from $N \approx 6$ to $N \approx 15$ upon switching on the relativity; relativity thus favors 2D bonding.
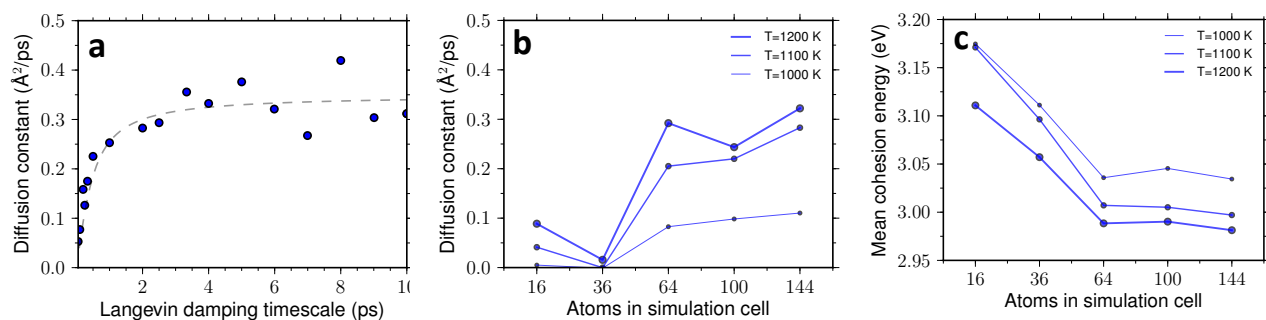
Fig. S2. Convergence of simulation parameters. (**A**) Diffusion constant as a function of Langevin damping time for Au_{64} at 1300 K and 4 % area strain. Dashed line is a sketch for a general trend. (**B**) Diffusion constant as a function of simulation cell size at three temperatures. (**C**) Mean cohesive energy per atom as a function of cell size at three temperatures.
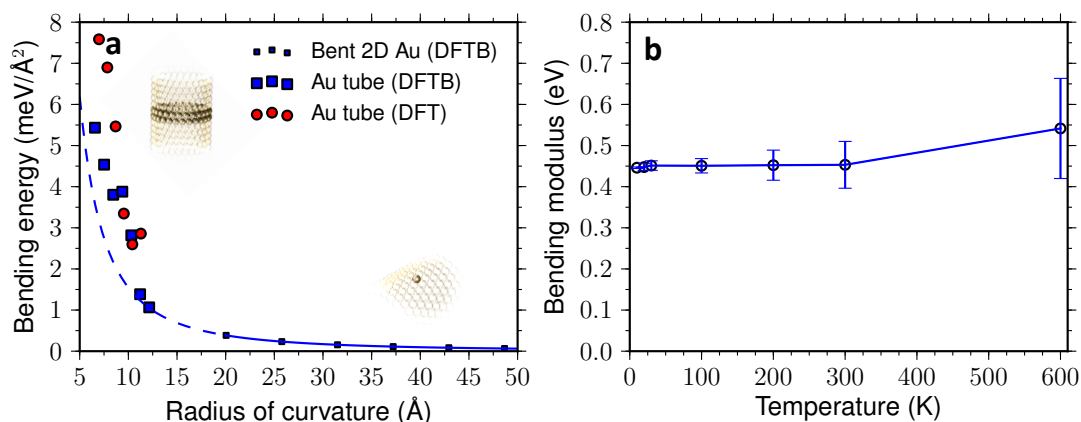

Fig. S3. Bending rigidity of 2D Au. (**A**) Bending energy as a function of radius of curvature for bent 2D Au (lower inset; one atom in unit cell using RPBC approach) and Au tubes (upper inset; $28 - 52$ atoms in unit cell). A fit above 20 Å yields bending modulus of 0.45 eV (solid line). Extrapolation below 20 Å (dashed line) gives a rough agreement with small-diameter tubes. (**B**) Bending modulus of 2D Au as a function of temperature (Au_{64} RPBC simulations with DFTB). Errorbars are from the error analysis of fitting.
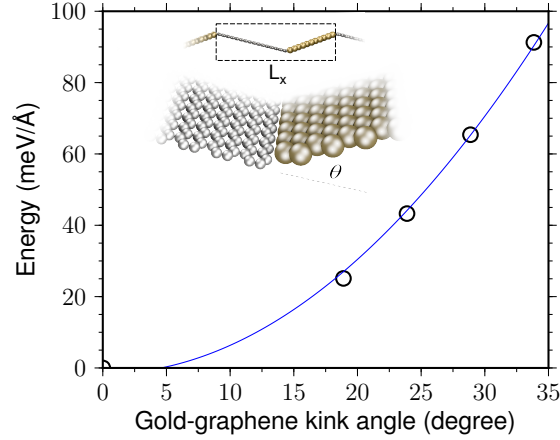
Fig. S4. Bending rigidity of Au-C interface. Plot shows the energy density of one Au-C interface as a function of the kink angle θ, as calculated by decreasing the length L_x of a periodic cell that contains two rigid bodies made of Au and C slabs (C: length 3.2 nm; Au: length 2.1 nm; width 2.5 Å; 1×6 k-point sampling). By normalizing the energy to the surface area of the interface, one obtains bending modulus of $\kappa_{Au-C} = 0.54$ eV (solid line), essentially the same as that of 2D Au (Fig. S3).
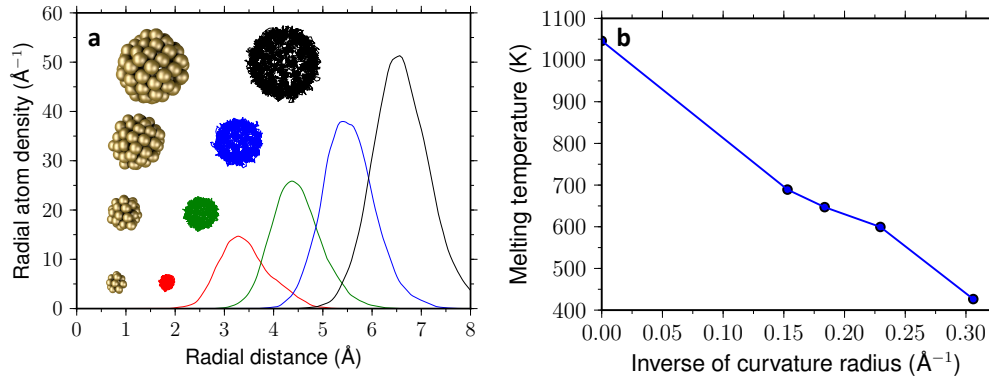

Fig. S5. Effect of curvature on melting temperature. (**A**) Radial atom densities of gold cages averaged over 50 ps simulations showing the cavities in the centers of mass. Clusters have 18, 32, 50, and 72 atoms. Insets: snapshots and atom trajectories. (**B**) Melting temperature as a function of inverse of curvature radius. The criterion for liquid was $D > 0.1$ Å^2/ps; the melting temperature at zero curvature was adopted from 2D Au simulations.

References:

43.   J. P. J. Perdew, K. Burke, M. Ernzerhof, Generalized gradient approximation made simple. *Phys. Rev. Lett.* **77**, 3865 (1996).

44.   J. J. Mortensen, L. B. Hansen, K. W. Jacobsen, Real-spage grid implementation of the projector augmented wave method. *Phys. Rev. B.* **71**, 35109 (2005).

45.   J. Enkovaara *et al.*, Electronic structure calculations with GPAW: a real-space implementation of the projector augmented-wave method. *J. Phys.: Condens. Matter.* **22**, 253202 (2010).

46.   R. M. Martin, *Electronic structure: Basic Theory and Practical Methods* (Cambridge University Press, 2004).

47.   D. Porezag, T. Frauenheim, T. Köhler, G. Seifert, R. Kaschner, Construction of tight-binding-like potentials on the basis of density-functional theory: application to carbon. *Phys. Rev. B.* **51**, 12947 (1995).

48.   P. Koskinen, V. Mäkinen, Density-functional tight-binding for beginners. *Comput. Mater. Sci.* **47**, 237–253 (2009).

49.   M. Elstner *et al.*, Self-consistent-charge density-functional tight-binding method for simulations of complex materials properties. *Phys. Rev. B.* **58**, 7260 (1998).

50.   D. Frenkel, B. Smit, *Understanding molecular simulation. From Algorithms to Applications* (Academic Press, 2002).

51.   P. Koskinen, O. O. Kit, Efficient approach for simulating distorted materials. *Phys. Rev. Lett.* **105**, 106401 (2010).

52.   O. O. Kit, L. Pastewka, P. Koskinen, Revised periodic boundary conditions: fundamentals, electrostatics and the tight-binding approximation. *Phys. Rev. B.* **84**, 155431 (2011).

53.   https://trac.cc.jyu.fi/projects/hotbit.

54.   M. P. Johansson, D. Sundholm, J. Vaara, Au32: A 24-Carat golden fullerene. *Angewandte Chemie.* **43**, 2678–2681 (2004).

55.   S. Bulusu, X. Li, L. Wang, X. C. Zeng, Evidence of hollow golden cages. *PNAS.* **103**, 8326 (2006).